Journal of Molecular Liquids 384 (2023) 122190

Contents lists available at ScienceDirect

Journal of Molecular Liquids

journal homepage: www.elsevier.com/locate/molliq

Antineoplastic effect of paclitaxel-loaded polymeric nanocapsules on malignant human ovarian carcinoma cells (SKOV-3)

Moein Golshan Ara [a], Gholamreza Motalleb [b,*], Brenda Velasco [c], Abbas Rahdar [d], Pablo Taboada [c,*]

[a] Division of Cell and Molecular Biology, Department of Biology, Faculty of Science, University of Zabol, Zabol, Islamic Republic of Iran
[b] Division of Cell and Molecular Biology, Department of Biology, Faculty of Science, University of Zabol, Zabol, Islamic Republic of Iran
[c] Colloids and Polymers Physics Group, Particle Physics Department and Institute of Materials (IMATUS); Universidade de Santiago de Compostela, 15782 Santiago de Compostela, Spain
[d] Department of Physics, University of Zabol, Zabol, Islamic Republic of Iran

ARTICLE INFO

Keywords:
Ovarian cancer
Polymeric nanocapsules
Paclitaxel
Apoptosis
Oncogenes
Caspases

ABSTRACT

Drug resistance is the main responsible for chemotherapy failure in ovarian cancer treatment. In this study, we looked at increasing the anticancer effect of paclitaxel (PTX) through its encapsulation in novel polymeric nanocapsules to develop a novel, less invasive PTX-loaded nano-delivery system. These were synthesized by a microemulsion-based methodology, and their particle size and shapes determined using dynamic light scattering (DLS) and field emission scanning electron microscopy (FESEM). The synthesized PTX-loaded polymeric nanocapsules showed spherical morphology with approximately ca. 18 nm. *In vitro* cytotoxicity analysis of free administered PTX, bare and PTX-loaded polymeric nanocpasules by means of the MTT assay showed that much lower concentration of PTX loaded inside polymeric nanocapsules (2.2 μg/ml) were needed to achieve a similar therapeutic activity than the free administered drug (14.4 μg/ml). Polymer nanocapsule encapsulation of PTX then improved the therapeutic efficacy as shown by the reduction of IC50 concentration. *MYC*, *MECOM*, *PRKCl* gene and caspases-3, −8, and −9 protein expressions involved in the apoptotic pathway after the treatment of SKOV-3 cells with PTX-loaded polymeric nanocapsules were assessed by qRT-PCR and fluorometric assay, respectively. The expression level of *MECOM* increased 1.67 times upon administration of PTX-loaded polymeric nanocapsules compared with untreated SKOV-3 cancer cells as the control group ($P < 0.001$); conversely, *MYC* and *PRKCl* gene expressions were 0.40 and 0.45 times lower compared to control cancerous cells ($p < 0.001$). The expression of caspase-3, caspase-8, and caspase-9 proteins also significantly increased after the administration of PTX-loaded polymeric nanocapsules to cancer cells ($p \leq 0.001$). On the other hand, fluorescence microscopy analysis showed nuclei fragmentation after administration of 24.1 μg/mL of PTX-loaded polymeric nanocapsules, which is accompanied by morphological cell alterations, confirming the cytostatic activity of the nanoformulation. Therefore, the synthesized PTX-loaded polymer nanocapsules could be promise and potential nano-delivery system for PTX delivery in ovarian cancer chemotherapy.

1. Introduction

Cancer is becoming the second cause of death worldwide after cardiovascular diseases, with 13 million cancer deaths and more than 21 million new cases predicted globally by 2030 [1]. Amongst the different types of tumors, ovarian cancer ranks the fifth most fatal for females. The risk of suffering an ovarian cancer throughout womeńs life is 1 out of 78 whereas the risk of death ca. 1 out of 108, consequence in many cases of the insufficient efficacy of current therapies [2], for which paclitaxel and cisplatin are the two main standard-of-care drug-based treatments [3]. Ovarian cancer is considered to involve multiple genomic reorganizations, part of which still remains unknown [4]. What it is clear is that the bad prognosis and relatively high mortality of this type of cancer is directly related to the development of drug resistance mechanisms upon treatment [5]. These are mainly related to the molecular activity and expression of drug efflux pumps, altered pH of

* Corresponding authors..
E-mail addresses: mgolshan98@yahoo.com (M.G. Ara), reza.motaleb@uoz.ac.ir (G. Motalleb), rezamotalleb@gmail.com (B. Velasco), a.rahdar@uoz.ac.ir (A. Rahdar), pablo.taboada@usc.es (P. Taboada).

https://doi.org/10.1016/j.molliq.2023.122190
Received 14 March 2023; Received in revised form 12 May 2023; Accepted 23 May 2023
Available online 26 May 2023

tumoral cells, deficient DNA damage repair capacity, and methylation of different genes [6]. However, other processes such as insensitivity to drug-induced apoptosis and stimulation of drug-detoxifying mechanisms might also largely contribute to decrease the efficacy of chemotherapy to treat this cancer [7]. Advanced ovarian cancer is also affected by extensive oncogene alterations amongst which the *MYC* oncogene amplification occurs in approximately half of tumors, thus, being considered a potential therapeutic target for ovarian cancer therapy [8] and one of the seven major driver cancer genes identified in a genomic landscape investigation of breast cancer [9]. Previous studies also showed that *MECOM* and *PRKCI* are growth-promoting genes largely expressed in ovarian cancer [4]. *MECOM* gene (also known as ecotropic virus integration site 1, EVI1) encodes a zinc finger protein that plays a role as a transcription factor [10–12] whilst *PRKCI* gene encodes protein kinase C iota (PKCi) enzyme, a member of the protein kinase C family and an oncogenic K-Ras effector protein [13–15].

Paclitaxel (PTX) is a potent anticancer drug with a diterpenoid pseudoalkaloid structure [16] which has been accepted by the US Food and Drug Administration (FDA) as first line treatment of both ovarian and breast cancers. Nevertheless, administration of PTX is challenging due to its negligible bioavailability [16]. Numerous nanoformulations to solve this issue and then decrease potential adverse side effects of this drug have been developed and analyzed such as nanoparticles, liposomes, microspheres and nanosponges [16]. In this regard, nanocapsules are vesicular structures including a polymeric membrane that encloses an inner liquid core [16] and have been widely studied as a potential drug delivery system in recent years. Nanocapsules—as one of kind nanoparticle— have a unique nanostructure, consisting of a liquid/solid core with a polymeric shell with sizes ranging from 10 nm up to 1000 nm [17], and may provide extraordinary permeability and drug solubility enhancements as well as improving bioavailability whilst reducing harmful side effects [18,19]. Compared with solid polymeric nanospheres, the solid/oil core of nanocapsules can effectively increase the drug-loading efficiency, while reducing the polymeric matrix content of nanoparticles [20]. In this regard, both lipo-polymer and Pluronic F127 polymeric-based nanocapsules have been used to successfully load PTX into their cores. For example, a Pluronic F127-based nanoformulation was able to inhibit tumor cell growth and reduced IC50 compared to free PTX administration [21]. However, a deep analysis of the antineoplastic effect of PTX-loaded Pluronic F127 polymeric nanocapsules on ovarian cancer has not been investigated yet and, in particular, our focus is on understanding how PTX-loaded polymeric nanocapsules affect *MYC*, *MECOM*, *PRKCl* genes and caspases-3, −8, and −9 protein expressions involved in the cell apoptotic pathway after treatment administration. In this study, the chemotherapeutic activity of the drug PTX was investigated upon its encapsulation within small polymeric nanocapsules to develop a novel, less invasive, PTX nanodelivery system against malignant SKOV-3 human ovarian carcinoma cells. Our *in vitro* cytotoxicity data revealed that lower concentrations of PTX-loaded polymeric nanocapsules lead to similar cytotoxic activity as compared to the free drug alone. Our results showed that 1 μg/mL polymer nanocapsules reduced the IC50 of PTX from 14.4 to 2.2 μg/mL during the first 72 h. Interestingly, PTX-loaded polymer nanocapsules significantly increased apoptosis via caspase-dependent pathways as well as cytoskeletal structure disruptions in SKOV-3 cancer cells.

2. Materials and methods

2.1. Materials

Dulbecco's modified Eagle's medium (DMEM, high glucose, Caisson, Smithfield, USA), PTX (Rooyan Darou, Tehran, Iran), fetal bovine serum (FBS) (Gibco, Paisley, UK), 3-[4,5-dimethylthiazol-2-yl]-2,5-diphenyl tetrazolium bromide (MTT) (Sigma-Aldrich, USA), sodium chloride (Merck, Germany), disodium hydrogen phosphate (Merck, Germany), potassium dihydrogen phosphate (Merck, Germany), potassium chloride (Sinchem, South Korea), Pluronic F127 (BASF, New Jersey, USA), sodium caprylate (Sigma, St. Louis, USA), ethyl butyrate (Sigma, St. Louis, USA); potassium phosphate monobasic (Fisher Scientific Inc. Suwanee, GA),and potassium phosphate dibasic (Fisher Scientific Inc. Suwanee, USA) were of the highest purity level and used as received. On the other hand, malignant human ovarian cancer cell line (SKOV-3) was purchased from Pasteur Institute (C209, ATCC number HTB-77, Tehran, IR). Cells were cultured in DMEM containing 10 % (v/v) fetal bovine serum (FBS (Gibco, Paisley, UK) with 0.2 % gentamicin at 37 °C under 5 % CO_2-95 % air atmosphere with 70–80 % humidity.

2.2. Preparation of PTX-loaded polymeric nanocapsules

Preparation of PTX-loaded polymeric nanocapsules was carried out as described elsewhere [22–24]. PTX-loaded polymeric nanocapsules were obtained by dissolving 0.04 g of PTX in an 1 % (w/w) ethyl butyrate oil solution containing sodium caprylate (0.08 g); next, F127 (0.009 g) in phosphate-buffered saline (PBS, pH 7.4) in an ethyl butyrate:Pluronic F127 molar ratio of 1 were added and the resulting solution (10 mL) vigorously stirring at room temperature. The made PTX-loaded polymer nanocapsules were kept for 4 months in order to test their colloidal stability. A scheme of the PTX-loaded polymeric nanocapsules is shown in Fig. 1.

2.3. Dynamic light scattering (DLS) and field emission scanning electron microscopy (FESEM) of PTX-loaded polymer nanocapsules

DLS was carried out to measure the size of PTX-loaded and bare polymeric nanocapsules using an ALV-5000F Goniometer System (Sartorius, Germany) coupled with a diode-pumped solid-state laser to supply polarized incident light as described elsewhere [25,26]. The system was combined with a digital correlator (ALV SP-86, 25 ns to 100 ms). DLS was carried out at an angle of $\theta = 90^{\circ}$. The hydrodynamic diameter of nanocapsules was calculated according to the Stokes-Einstein relationship [26]. The size of nanomicelles can be characterized according to the Stokes-Einstein equation [23,24]:

$$R_h = \frac{k_B T}{6\eta\pi D} \tag{1}$$

where T is the temperature in K, η is the viscosity of the continuous phase, and K_B is Boltzmann's constant.

Particle morphology was also analyzed by field emission scanning electron microscopy (Tescan Mira3, Czech Republic). To do that, the solution sample was deposited on aluminum foil and vacuumed, then covered with a thin gold layer by sputtering and imaged.

2.4. Drug encapsulation efficiency

The encapsulation efficiency (EE%) of PTX-loaded nanocapsules was evaluated by UV–vis spectroscopy (Shimadzu UV-1700 PharmaSpec, Kyoto, Japan), following the method described by Rahdar et al. [27] In this regard, PTX-loaded nanocapsules were centrifuged at 20000 rpm for 60 min. The concentration of PTX in the supernatants was determined by absorbance at 227 nm. Finally, the PTX concentration was calculated by a standard calibration curve, and the EE% calculated using the following equation:

$$Encapsulation\ efficiency\ (EE\%) = \frac{\left([PTX]_{total} - [PTX]_{free}\right)}{[PTX]_{total}} \times 100 \tag{2}$$

where $[PTX]_{total}$ and $[PTX]_{free}$ is the concentration (mass) of drug initially fed and not incorporated in the nanocarrier, respectively.

The drug loading (DL%) was calculated as follows:

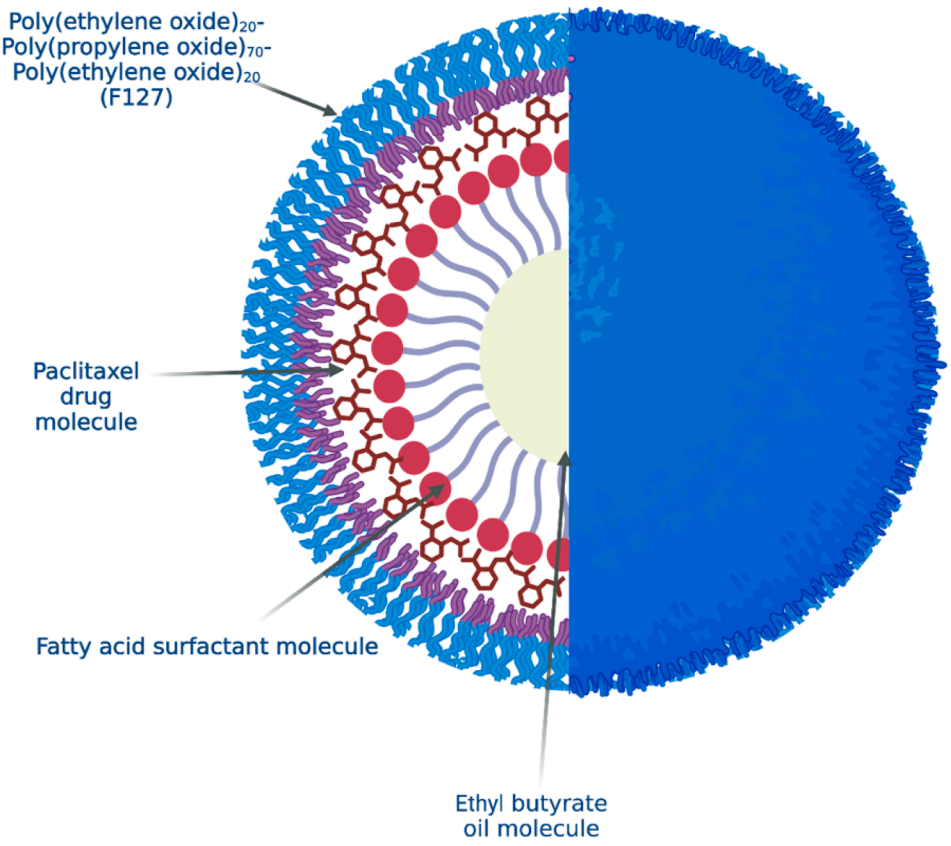

Fig. 1. Scheme of PTX-loaded polymer nanocapsules (Figure created with Biorender).

$$Drug\ loading\ (DL\%) = \frac{\left([PTX]_{total} - [PTX]_{free}\right)}{[nanocapsules]} \times 100 \quad (3)$$

where [nanocapsules] is the mass of the nanocarriers containing the drug.

2.5. Drug release

PTX release profiles for free PTX and PTX-loaded nanocapsules were determined by dialysis experiments using a 10 kDa cut-off dialysis membranes. Accordingly, a certain amount (1 mL) of free drug and drug-loaded nanovehicles was poured into 10 kDa dialysis membranes. The dialysis bags were immersed in 50 mL of PBS (pH 7.4) and incubated in a shaker incubator at 37 °C (90 rpm). At different time points, 100 μL of the sample solution were transferred to a test tube and replaced with 100 μL of fresh PBS solution. The concentration of released PTX was assessed by UV spectrophotometry (Shimadzu UV-1700 PharmaSpec, Kyoto, Japan) at 227 nm. Finally, the concentration of PTX at each time point was evaluated by a standard calibration curve and expressed as the percent of cumulative drug released.

2.6. MTT cytotoxicity assay

SKOV-3 cancer cells were cultured at 1×10^4 cells/well on 96-well plates with DMEM supplemented with 10 % (v/v) FBS and incubated in an 80 % humidified-5 % CO_2 atmosphere at 37 °C. Selection of dosages was done to cover a wide range of drug concentrations from below to highly exceeding the currently used therapeutic concentrations. Cells were then treated with free PTX (2, 4, 8, 16, 31, 62, 125, 250, and 500 μg/mL), bare polymeric nanocapsules (equivalent PTX concentration of 3.6, 7.2, 14.3, 28.7, 57.3, and 114.7 μg/mL), and PTX-loaded polymeric nanocapsules (final PTX concentration of 3.0, 6.0, 11.9, 23.8, 47.6, 95.3, and 190.5 μg/mL), and their cytotoxic effect evaluated by means of the (3-[4,5-dimethylthiazol-2-yl]-2,5-diphenyl tetrazolium bromide) (MTT) assay [27,28] after 24 and 72 h of incubation. Differences in concentrations arose from the real quantification of the drug presence in solution and not from estimates. The MTT reagent solution was made by dissolving 5 mg of MTT in 10 mL of PBS. Then, at suitable time points, 100 μL of MTT (0.5 mg/mL) reagent (Sigma, St Louis, MO, USA) were added to each well. The plates were incubated for 4 h in an 80 % humidified-5 % CO_2 atmosphere incubator at 37 °C. Then, MTT reagent was eliminated and 100 μL isopropanol added to each well. The plates were incubated for 5 min until the formazan crystals dissolved, and the absorbance at 570 and 630 nm was measured with a microplate reader (Bio-Rad, Hercules, CA, USA). Cell viabilities were presented as the % survival rate, using the following equation [29]:

$$Survival\ rate\ (\%) = \left(\frac{\left[\frac{A_{well(570nm)} - A_{blank(570nm)}}{A_{well(630nm)} - A_{blank(630nm)}}\right]}{\left[\frac{A_{control(570nm)}}{A_{control(630nm)}}\right]} \right) \times 100 \quad (4)$$

where A refers to the absorbance, and the subscripts well, blank and control to the absorbance of sample, negative control and positive control, respectively.

2.7. RNA extraction and cDNA synthesis

Total RNA extraction and cDNA synthesis was carried out using the EasyPure® RNA Kit (TransGene Biotech, China) and EasyScript® First-Strand cDNA Synthesis SuperMix Kit (TransGene Biotech, China), respectively, according to the manufactureŕs instructions. Briefly, the prepared cell suspension ($<5 \times 10^6$ cells) was transferred to a RNase free test tube and then centrifuged at 12000 × g (5 min). Next, cells were lysed by binding buffer 4 (BB4). Then, the cell pellet was homogenized at 12000 × g for 5 min. Finally, the RNA purification was carried out at room temperature according to the kit manufactureŕs instructions. Total

RNA was used for synthesis of cDNA. For that, anchored oligo $(dT)_{18}$ primer was incubated at 42℃ for 30 min, and then finally incubated at 82℃ for 5 s to inactivate enzymes.

2.8. SYBR green real-time PCR

The expression levels of *MYC*, *PRKCl*, and *MECOM* genes were evaluated using an Applied Biosystems StepOne™ Real-Time PCR System (Thermofisher Scientific, USA) and TransStart® Green qPCR SuperMix Kit (TransGene Biotech, China). Briefly, the synthesized cDNA was subjected to SYBR green real-time PCR. Glyceraldehyde-3-phosphate dehydrogenase (GAPDH) was used as the housekeeping gene. RT-qPCR conditions are shown in Table 1. The genes expression levels were calculated by means of the $2^{-\Delta\Delta Ct}$ method [30]. All primers were automatically designed by Primer3 package [31,32]. Next, the primer specificity was further predicted by using the online tool Primer-BLAST [33].

2.9. Measurement of apoptosis by caspase-3, −8, and 9 protein expressions.

According to manufacturers ' instructions, the colorimetric assay of caspases-3, −8, and −9 activities was carried out using the Caspase Substrate Assay Kit (Abnova, Taipei, Taiwan). This was done to quantify the caspase enzyme activity by recognizing the amino acid sequences, Ac-DEVD-pNA (for caspase-3), Ac-IETD-pNA (for caspase-8), and Ac-LEHD-pNA (for caspase-9), respectively. Briefly, SKOV-3 cells were treated with 24.1 μg/mL of PTX-loaded nanocapsules for 24 h. Next, cells (5×10^5 per sample) were collected and added to 50 μL lysis buffer on ice for 10 min. Following centrifugation at 10.000g for 1 min, the lysate was collected and stored at −20 °C until further use. The quantification was made by measuring the absorbance at ca. 400–405 nm in an ELISA reader (Perlong, MR-960, China).

2.10. Cell morphological evaluation by fluorescence microscope

The morphological changes of SKOV-3 cells after treatment were carried out as described elsewhere [34]. Briefly, SKOV-3 cells (5×10^5 cells) were treated with PTX-loaded polymeric nanocapsules at a concentration of 24.1 μg/mL for 24 h in 6-well plates, and subsequently collected and fixed at 4 °C for 20 min. Cells were then stained with Hoechst 33,342 in the dark for 5 min, followed by washing three times with PBS. Finally, the morphological changes of SKOV-3 cells were observed by fluorescence microscopy (Optika, B-500TiFL, Italy).

Table 1
Sequence of the primers designed for real time PCR assay.

Primer	Sequence (5′→3′)	Condition	Product size(bp)
MYC: F *MYC*: R	AGACAGATCAGCAACAACCGAA ACAAGAGTTCCGTAGCTGTTCA	95℃ for 10 min, 40 Cycles: 95℃ for 15 s, 60℃ for 1 min Melt curve: 95℃ for 15 s, 80℃ for 1 min, 95℃ for 15 s	314
PRKCl: F *PRKCl*: R	ACGGCATGTGTAAGGAAGGATT TGTGTTCTGGTCAGGGTTATCG	95℃ for 10 min, 40 Cycles: 95℃ for 15 s, 60℃ for 1 min Melt curve: 95℃ for 15 s, 80℃ for 1 min, 95℃ for 15 s	209
MECOM: F *MECOM*: R	TAATTCGCCACCAGATGTCACA CTGTGGATGTGCTTGTGTTGTT	95℃ for 10 min, 40 Cycles: 95℃ for 15 s, 60℃ for 1 min Melt curve: 95℃ for 15 s, 80℃ for 1 min, 95℃ for 15 s	195

Abbreviations: F = forward; R = reverse.

2.11. Statistical analysis

All data were reported as a mean ± standard deviation and analyzed with SPSS software version 28.0.1 (SPSS Inc., USA). Each measurement was the mean of three different replicates. Statistical significance was calculated using Student's *t*-test for the comparison of two groups, and one-way analysis of variance (ANOVA) to assess multiple groups [35]. *P < 0.05 was considered statistically significant, **P < 0.01 very statistically significant and ***P < 0.001 as extremely statistically significant.

3. Results

In the present study, we aimed to increase and improve the antitumoral efficacy of paclitaxel (PTX) through its encapsulation within polymeric nanocapsules to develop a novel, less invasive, PTX nano-delivery system against malignant human ovarian carcinoma cell.

3.1. Characterization of PTX-loaded polymeric nanocapsules.

The homogenous PTX-loaded polymeric nanocapsules were prepared by a microemulsion-based method. Fig. 2A and B display the autocorrelation function and the hydrodynamic size population distribution of the PTX-loaded polymeric nanocapsules, respectively, which have a hydrodynamic diameter of ca. 18 ± 1 nm. The lack of tail at long delay/sampling times and the existence of narrow porpulation distribution confirmed the homogeneous character of the nanocapsule sizes. The particle size is largely maintained upon incubation for long periods of time (see Fig. 2C), without signs of either aggregation or precipitation (Fig. 2D), denoting the stability of the formulation. The morphology of polymeric nanocapsules was also observed by FESEM after 4 months of storage. As shown in Fig. 2E, polymeric nanocapsules retained their spherical shapes, with a mean diameter size of ca. 23 ± 4 nm. It is worth mentioning that the size obtained by FESEM is rather similar as that obtained by DLS; nevertheless, some little particle swelling may occur upon storage due to water penetration inside the nanocapsule, as observed from Fig. 2C but the colloidal stability and maintenance of particle morphology was completely maintained as mentioned previously.

On the other hand, the encapsulation efficiency of PTX inside the present polymeric nanocapsules was ca. 83.8 ± 4.7 % and the drug loading ca. 1.8 ± 0.6 %, respectively, even better than those obtained in some previous studies [36]. In addition, Fig. 2F shows the release profile of PTX encapsulated in the polymeric nanocapsules and of free drug calculated as the accumulative PTX release from dialysis experiments. The release profile of free PTX showed that ca. 100 % of the drug was released just after 4 h of incubation. Meanwhile, PTX released from polymeric nanocapsules showed a much slower release kinetics with an initial burst phase within ca. the first five hours of incubation, in which up to ca. 38 % of the drug was released and then, it leveled off to reach ca. 47 % of total drug after 48 h of incubation [37–39].

3.2. Cytotoxicity of PTX-loaded polymeric nanocapsules in SKOV-3 cancer cells.

Cytotoxicity assays confirmed that the developed nanocapsules were non-toxic to cells (see Fig. 3). Data showed that the half-maximal inhibitory concentration (IC50) was 9.5 and 24.1, and 14.4. and 2.2

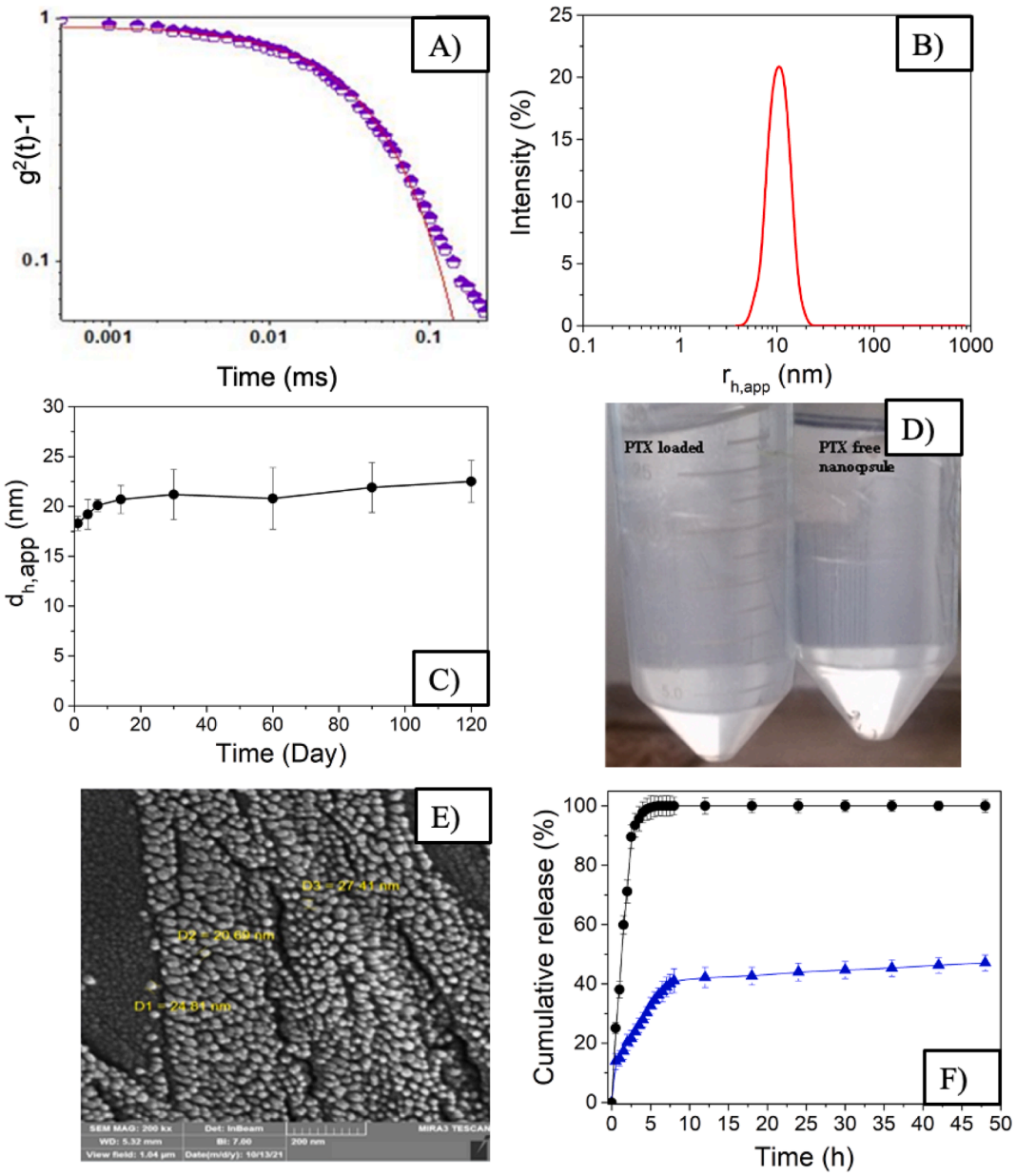

Fig. 2. A) DLS autocorrelation function of PTX-loaded polymer nanocapsules. B) Size distribution population of PTX-loaded nanocapsules obtained by DLS. C) Size evolution of PTX-loaded polymeric nanocapsules upon incubation. D) Image of PTX-loaded polymeric nanocapsules after 4 months of storage. E) FESEM image of bare polymeric nanocapsules after 4 months of storage. F) Release profiles of (●) free PTX and (▲) encapsulated inside the nanocapsules at pH 7.4 and 37 °C (n = 3).

μg/mL after the administration of free PTX and PTX-loaded polymer nanocapsules after 24 and 72 h of incubation, respectively. Hence, the encapsulation of PTX inside the polymeric nanocapsules seems to enhance the drug efficacy as indicated by the decrease in IC50 concentration [36].

3.3. Evaluation of caspase-3, −8 and −9 activities.

The caspase-3, −8, and −9 proteins expressions and activities after treating SKOV-3 with PTX-loaded polymeric nanocapsules were evaluated. The expression of these proteins significantly increased after the administration of the drug-loaded polymeric nanocarrier compared to untreated SKOV-3 ones used as the control group ($p \leq 0.001$) and to free administered drug (Fig. 4), that is, the administration of the PTX-loaded nanovehicle significantly increased the apoptotic pathway as a consequence of its reinforced chemotherapeutic activity.

3.4. Effect of PTX-loaded polymer nanocapsules on MYC, MECOM and PLAU gene expressions in SKOV-3 cancer cells

For the first time, developed qt-PCR experiments allowed to quantify the expression levels of genes related to the development of chemotherapy resistance in ovarian cancer. In this regard, interestingly, the expression level of *MECOM* increased 1.67 times for the PTX-loaded polymeric nanocapsules treated group compared with untreated SKOV-3 cancer cells as the control ($P < 0.05$) (see Fig. 5); conversely, the results showed that *MYC* and *PRKCl* gene expressions were 0.40 and 0.45 times lower in SKOV-3 cancer cells treated with PTX-loaded polymer nanocapsules compared with untreated SKOV-3 cancer cells, respectively ($p < 0.001$).

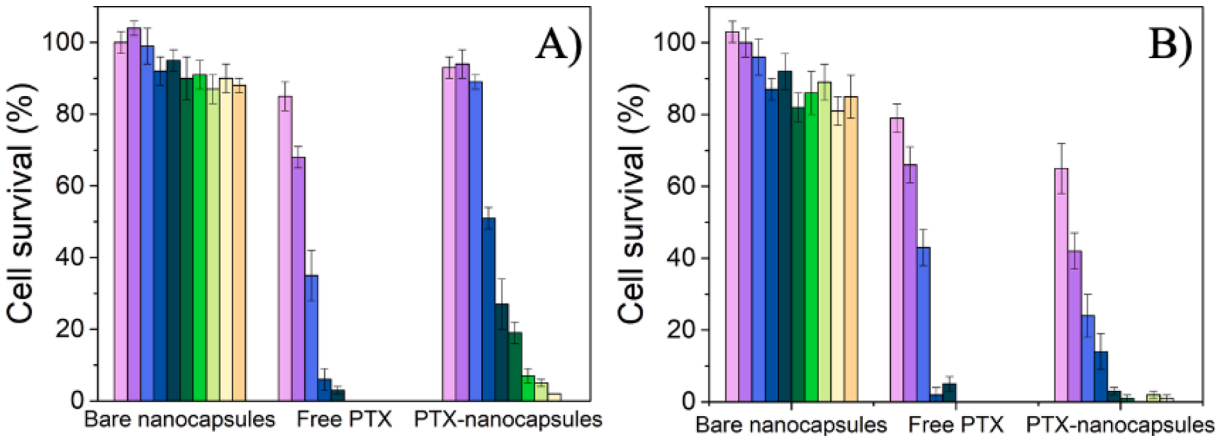

Fig. 3. Cytotoxicity of bare nanocapsules, free PTX and PTX-loaded polymeric nanocapsules in SKOV-3 cancer cells after A) 24 and B) 72 h of incubation, respectively. 2; 4; 8; 16 31; 62; 125; 200; 250; 500 μg/mL of PTX. For bare nanocapsules, an equivalent concentration similar as those containing PTX was administered.

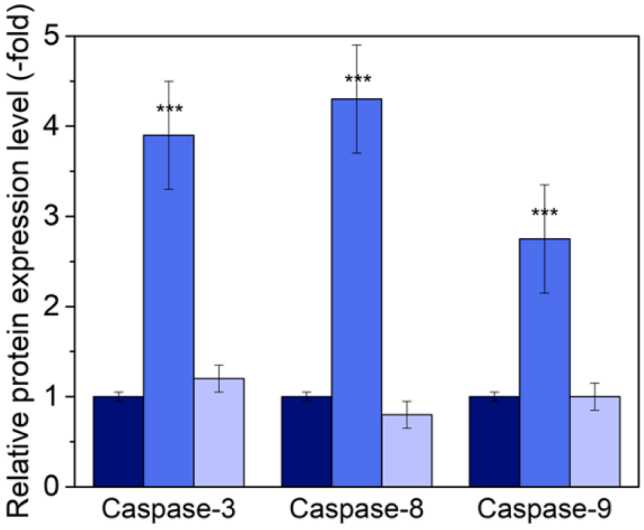

Fig. 4. Protein expression levels of caspase 3,8 and 9 in SKOV-3 cancer cells treated with PTX-loaded polymeric nanocapsules at a dose of 24.1 μg/mL (*** $P < 0.001$) . Control cells; free PTX; PTX-loaded nanocapsules.

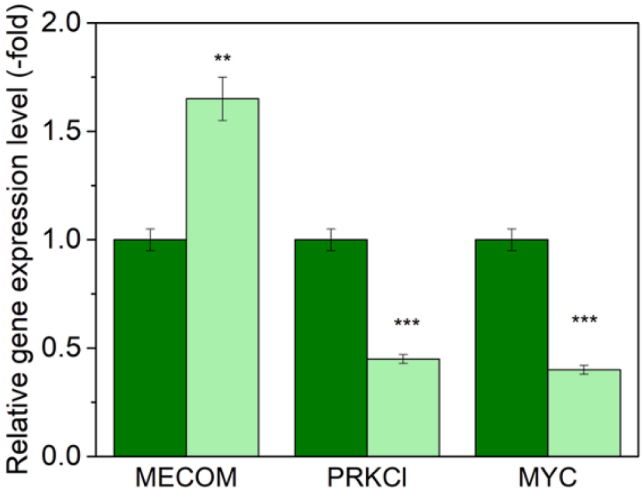

Fig. 5. Expression levels of *MECOM*, *PRKCl* and *MYC* genes in SKOV-3 cancer cells treated with 24.1 μg/mL of PTX-loaded nanocapsules. Means ± SD ** $P < 0.01$; *** $P < 0.001$. Control cells; PTX-loaded nanocapsules.

3.5. Morphological changes in malignant ovarian carcinoma cells after drug-loaded nanovheicle administration

After treatment with free PTX and PTX-loaded polymeric nanocapsules, potential morphological alterations of the cancerous cells were examined under light microscopy. Fig. 6 shows images of cells treated with free PTX, with PTX-loaded polymeric nanocapsules, and cells exposed to bare polymeric nanocapsules obtained by light (A) and fluorescent microscopy (B).

Fig. 6 confirmed that after treatment with 24.1 μg/mL of PTX-loaded polymeric nanocapsules morphological changes could be observed in the cell nuclei under fluorescence microscopy (Fig. 6B), whereas such an effect could not be discerned upon administration of bare polymeric nanocapsules. Interestingly, the observation of apoptosis features was observed PTX-loaded nanocapsule treated cells such as chromatin, nuclear and cytoplasmic condensations (Fig. 6B). Also, cell membrane blebbing and decrease of cell volume was also observed, which are characteristic features of the final stage of apoptosis, as confirmed in Fig. 6A. In this regard, stable and regular stained nuclei were observed with a less bright blue fluorescence in the untreated SKOV-3 cancer cells group (Fig. 6B). Light microscopy also revealed morphological alterations in PTX-loaded polymeric nanocapsules and free PTX-treated SKOV-3 cancer cells after 24 h of incubation (Fig. 6A). The cells began to round and lose their shape. At high concentration, these changes intensify, and many cells separate to form irregularly shaped masses. At much greater dosages, cell density dropped as consequence of cell death and detachment.

4. Discussion

In this study, we intended to enhance the anticancer effect of paclitaxel (PTX) by means of its encapsulation into polymeric nanocapsules to develop a novel, less invasive, PTX nano-delivery system against malignant human ovarian carcinoma cells (SKOV-3). The most common clinical treatment of progressive ovarian cancer is based on surgery followed by chemotherapy, for which the most effective and first-line

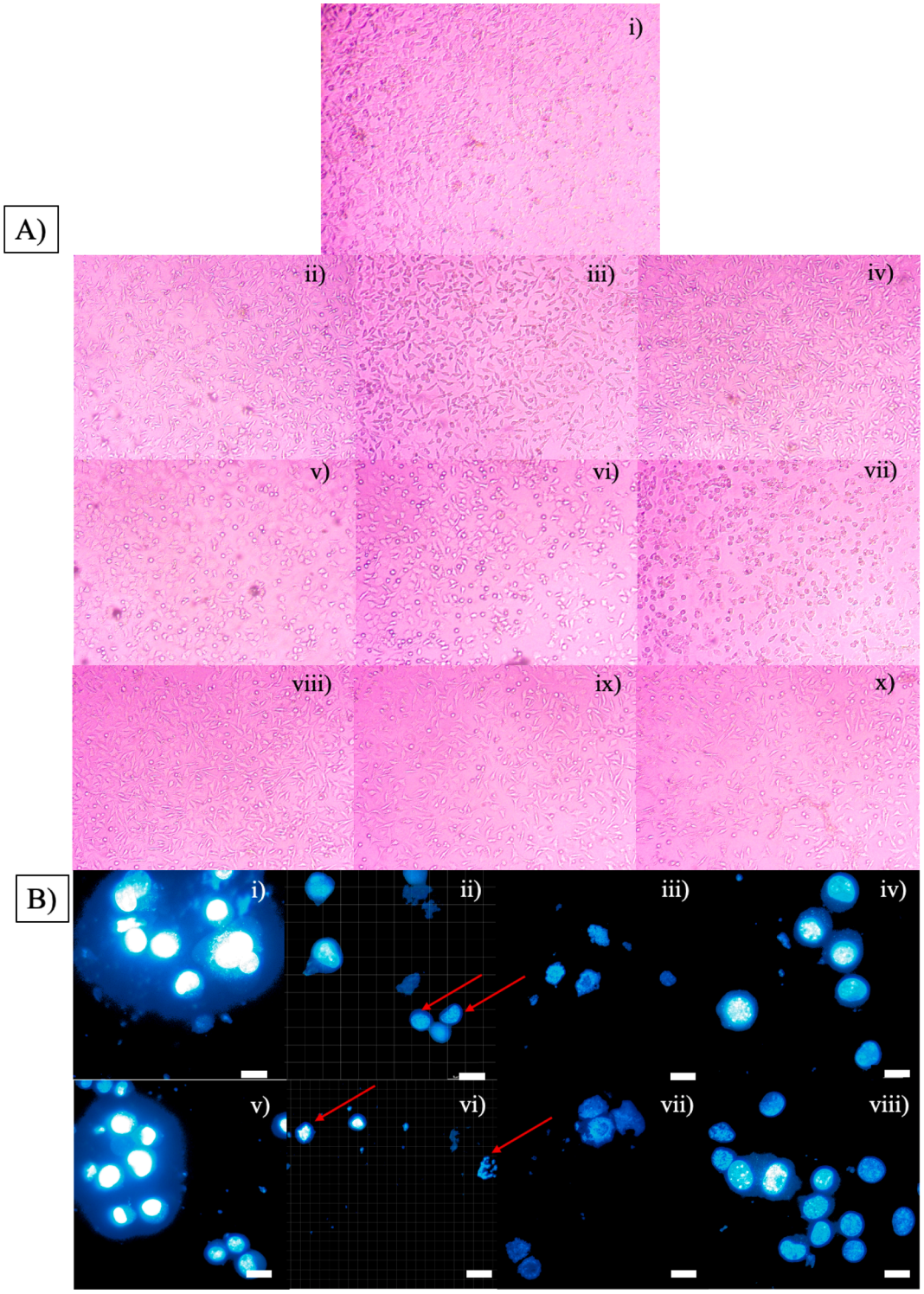

Fig. 6. A) Light microscopy images (magnification 20X). **ii-iv) Bare nanocapsules-treated; v-vii)** Free PTX-treated, and vii-x) PTX-loaded polymeric nanocapsules treated-cells at ca. 3.5, 7 and 14 μg/mL of drug, respectively. B) Fluorescent microscopy images of i,v) control cells; ii,vi) free PTX; iii,vii) PTX-loaded polymeric nanocapsules, and iv,viii) bare nanocapsules administered to cells. For free PTX-treated cells, red arrows denote fragmented and condensed nuclei, whereas for PTX-loaded polymeric nanocapsules nuclei morphology was observed to change.

drug therapies are carboplatin and paclitaxel. However, many patients experience severe side effects together with tumor recurrence as consequence of developed chemotherapy resistance [5]. Amongst the different drug delivery nanocarriers for paclitaxel, nanoparticles made of different biodegradable polymers such as chitosan, Pluronic F127, albumin, and gelatin have been tested [40] confirming enhancements of drug activity by modifications of its pharmacokinetics and pharmacodynamics. On the other hand, nanoparticles can prevent fast clearance of the drug by the reticuloendothelial system and can be accumulated in the tumor areas thanks to the defenestrated leaky vasculature of tumors (the so-called enhanced retention and permeation effect, EPR). In addition, multidrug resistance modulated, for example, by p-

glycoproteins can also be overwhelming through nanoparticle drug delivery systems. In this work, particle size and distribution of PTX-loaded polymer nanocapsules were detected by DLS, whereas their morphology checked by FESEM. Our results indicated that the hydrodynamic size of PTX-loaded nanocapsules was approximately 9 ± 1 nm. Interestingly, polymeric nanocapsules showed spherical shape with a mean size of around 24 ± 4 nm by FESEM after 4 months of storage, being still a suitable size to avoid renal excretion and favored accumulation in tumor by the EPR effect. [41,42]. In addition, the stability of the nanoformulation was also tested along time, and no signs of aggregation and precipitation were noted even after 4 months of storage. On the other hand, the present drug-loaded nanoformulation showed a 7-fold enhanced therapeutic efficiency when administered to SKOV-3 cancer cells compared to the administration of the free drug, much larger than that found in previous studies: For example, Levit *et al.* [36] when encapsulated PTX into tannic acid-modified PLGA NPs found a cell survival of ca. 80 % and only when combined with other drug (lapatinib) a synergistic effect was achieved by increasing cell death at ca. 50 % (combination index 0.23). In relation to this, MTT assay data showed that IC50 for free administered PTX and PTX-loaded polymer nanocapsules were 9.5 and 24.1 μg/mL and 14.1 and 2.2 μg/mL after 24 h and 72 h of incubation, respectively, that is, the toxic effect became stronger at longer incubation times. This observation is in agreement with the release profile of the drug from the nanocapsules observed in Fig. 2F, that is, the slower but sustained release of PTX allows a later achievement of the optimal therapeutic concentration but which can be kept along time; conversely, for the free administered drug this therapeutic threshold is rapidly reached but, then, the proper efflux mechanism of cells implied a fast decrease in the active drug concentration inside cells. Interestingly, bare polymer nanocapsules appeared safe and biocompatible with cells not displaying significant cytotoxicity.

Apoptosis is a kind of programmed cell death controlled by the Bcl-2 and proteins of caspases [43]. In particular, caspases play a central role in the regulation of apoptosis, and they are responsible for many biological and structural changes associated with this programmed cell death mechanism. Until now, 14 different caspases have been identified. All of them in the mature state form a head-to-tail dimer with each unit composed of a large and small subunit containing one active site. Upon activation, caspases begin to cleave a set of pre-defined substrates, ranging from a few to several hundred targets, at rates that can vary by over 500-fold between targets. In this regard, specific phenotypic outcomes are likely dependent on multiple factors including (i) which caspases are activated, (ii) which substrates are cleaved, (iii) the cellular context, and (iv) the post-activation regulatory machinery in the cell. Caspases have been categorized depending on the sequence similarity biological functions into three subclasses: Group 1 or caspase-1 subfamily (caspases-1, −4, −5, −11, −12 and −13) based on the commonalities of having a long caspase-recruitment domain and a preference for a large aromatic or hydrophobic residue at the *P*4 position; Group III or caspase-2 subfamily (caspases-2, −8 and −9, −10), which all contain a long pro-domain and prefer substrates with a leucine or valine at the *P*4 position; and Group II or caspase-3 subfamily (caspases-3, −6,-7) that share a similar short pro-domain, and play a role as 'executors of apoptosis' [43].

Particularly, caspase-9 is needed for mitochondrial structural alterations and ROS creation. After activation by caspase-9, caspase-3 prevents ROS production and is essential for the adequate performance of apoptosis. Previous studies demonstrated that caspase-8 could cut Bid into tBid, changing the mitochondria [43]. In the present study, a fluorometric assay allowed to quantify caspases-3, −8, and −9 proteins' expressions and activities after treatment of SKOV-3 with PTX-loaded polymer nanocapsules. Interestingly, our results showed that caspases 3, 8 and 9 proteins are significantly increased in PTX-loaded polymeric nanocapsules treated cancer cells compared to the control group ($P < 0.001$). However, the protein expression level of caspase 8 was higher than caspases-3 and −9. The present results agree with indicated the activation of caspase-3, −8, and −9 is the main pathway to induce apoptosis in SKOV-3 cells [44]. Amazingly, our results agree with those of Ahn et al. [44], who indicated that activation of caspase-3, −8, and −9 is the main pathway to induce apoptosis in SKOV-3 cancer cells.

High-grade serous ovarian cancer (HGSOC) involved an important amount of copy number aberrations (CNAs) that can lead to the amplification and silencing of oncogene and tumor suppressor genes, respectively. Gene amplifications have clinically predictive and symptomatic value because they have been confirmed as biomarkers to measure tumorigenic progression and drug resistance in cancer [45]. Chromosome 3q26 amplification is one of the most recurrent chromosomal modifications in ovarian and cervical human cancers. *PRKCl* is the main vulnerability locus within human chromosome 3q26, and is regularly amplified in ovarian cancer [46], and it has previously been shown as a possible and potential oncogene in ovarian cancer [45]. In this regard, Ren *et al.* [47] showed that PTX blocks the PI3K pathway, associated with $PRKC_l$ gene overexpression in ovarian carcinoma cells. In other words, proliferation and cell cancerous migration might decrease by inhibiting *PRKCl* gene expression levels. In addition, *MYC* oncogene is located in chromosome 8q24 and ovarian cancer shows the uppermost incidence of MYC amplification [8]. Our findings indicated that both *MYC* and *PRKCl* gene expression level decreased after administration of the drug-loaded nanovehicle up to levels of 0.40 and 0.45 times lower than in the case of the untreated control cell group. Previous studies indicated that PTX could cause arrested cells in G0-G1 and G2-M by stabilizing microtubules, inhibiting depolymerization and inducing apoptosis with the p53 signaling pathway [48,49]. As we found that *MYC* gene expression levels decreased upon drug-loaded nanocapsule administration, then, a potential mechanism of action of the delivery vehicle could be through the production of caspases-3, −8 and −9 as main effectors and executors of the apoptotic process as here observed, and the down-regulation of Bcl-2 cell survival family proteins, which play a key role in the tumoral cell survival signaling [50–54]. The reduction in *PRKCl* gene expression might be also related to the inhibition of the PI3K pathway, as shown in Fig. 7.

On the other hand, the *MECOM* gene, a transcription factor, is positioned on the human chromosome 3q26. The rearrangements of *MECOM* frequently causes its overexpression in acute myeloid leukemia (AML) and epithelial cancers. The *MECOM* gene play different roles associated with leukemogenesis, such as transcriptional control, regulation of signaling pathways, and the induction of epigenetic alterations [55]. SKOV3 cancer cells were used in our study since the *EVI1* gene is believed to be an ovarian carcinoma oncogene [56]. Interestingly, the expression level of *MECOM* increased upon administration of PTX-loaded polymer nanocapsules ($P < 0.05$). Mitani *et al.* showed that overexpression of *MECOM* is associated with JNK, c-jun, and anti-apoptosis mechanism [55,56]. *EVI-1* overexpression plays an essential role in (MAP) kinase pathway related to the apoptosis signaling pathway [57,58]. In other words, *EVI-1* inhibits JNK and c-jun interaction, therefore suppressing apoptosis induction. Amazingly, Jazaeri et al. reported that EVI1 protein expression patterns were similar amongst different ovarian cancers, fallopian tube fimbria, and benign neoplasms [11]. They showed that *MECOM* gene expression did not enhance proliferation in EVI1-null OVCAR8 cells. Hence, they did not verify a character for *EVI1* in ovarian cancer cell proliferation or response to DNA damage. So, we highly suggest additional studies to confirm *EVI1* as an oncogene or a therapeutic goal in ovarian cancer. Another study reported c-jun expression associated with *PRKCl* gene one in the PI3K pathway [59]. Thus, further studies are needed to understand the exact mechanism.

To additionally examine whether PTX-loaded polymeric nanocapsules stimulated apoptosis, SKOV-3 cancer cells were stained with Hoechst 33342. Hoechst 33,342 is a fluorescent dye that especially intercalates with nucleic acids in nuclei. The fragmented and shrinkage or condensed nuclei were observed under a fluorescent microscope and showed how the cells-initiated apoptosis. Our light microscopy findings

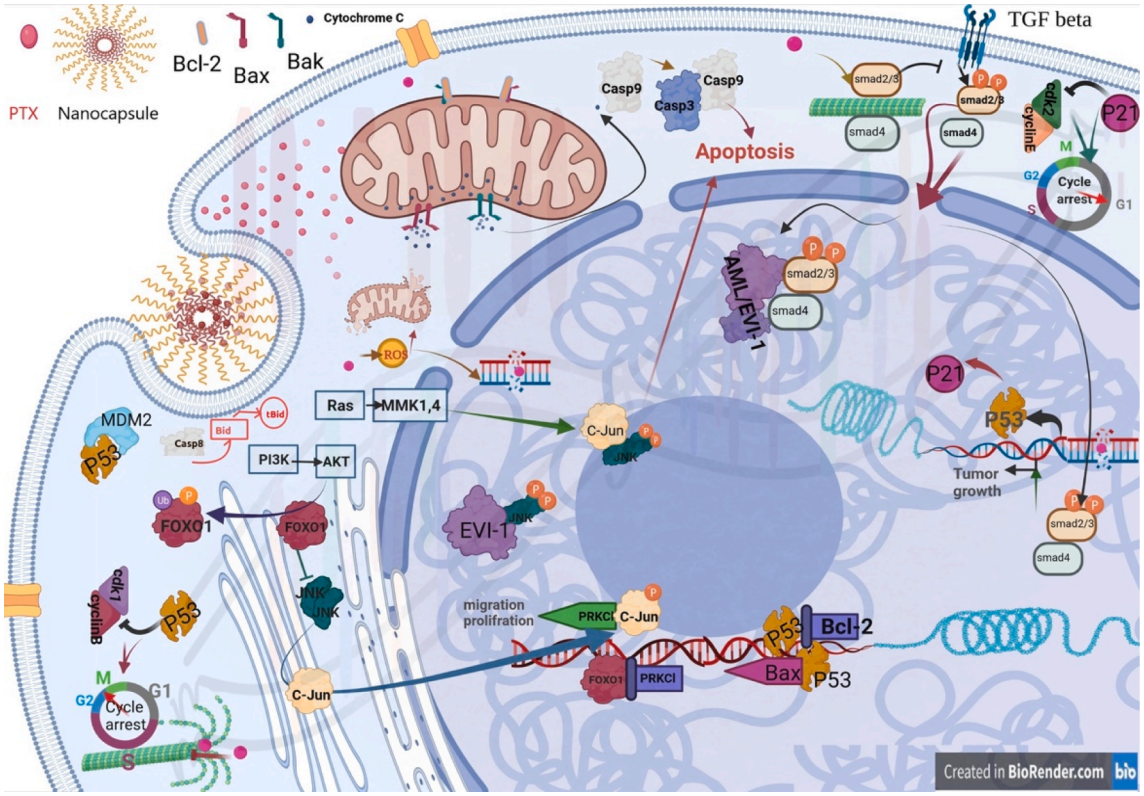

Fig. 7. The possible mechanism of apoptosis suggested for PTX loaded polymer nanocapsules. PTX involves oxidative stress by production of reactive oxygen species (ROS), which increases nicotinamide adenine dinucleotide phosphate (NADPH) oxidase [46,47]. Previous studies showed that PTX causes arrest cells at G0-G1 and G2-M by stabilizing microtubules and inhibiting depolymerization [47,60,61]. Thus, the P53 signaling pathway activates p53 by inhibiting cyclin-dependent kinases1 (CDK1), and cycling interaction induce apoptosis [62]. PTX also causes DNA damage, increasing P53 level and arrest cell at G1 phase cycle meditate with p21 [46]. Another possible mechanism for PTX could be PI3K/AKT pathway inhibition that is related to forkhead box protein O1 (FOXO1), Jun *N*-terminal kinase (JNK), c-jun witch impact on PRKCl expression level [47,63]. PTX) inactives Bcl-2 and activates Bax, Bak by phosphorylation and dephosphorylation respectively to stimulate apoptosis mediated by caspase 3, 9 [11,44,47]. Previous studies reported that p53 induces Bax and represses Bcl-2 transcription directly [64]. One pathway suggested PTX inhibit transforming growth factor-beta (TGF-β)/Smad signaling pathway, which plays a role in fibrosis and hematopoiesis [45,65]. Mitani showed that AML/EVI-1 inhibits apoptosis by interaction with Smad proteins in the TGF-β/Smad signaling pathway. Moreover, EVI-1 interferes in mitogen-activated protein (MAP) kinase cascades, including the JNK signaling pathway, preventing c-Jun/JNK interaction [55,57].

indicated that after 24 h of PTX-loaded polymeric nanocapsules administration, morphological alterations (many cells with irregularly shaped masses and reduced cell density) increased dramatically in SKOV-3 cancer cells. To summarize, our *in vitro* cytotoxicity findings suggest that the antiproliferative activity of PTX-loaded polymeric nanocapsules on SKOV-3 cancer cells was substantially higher than that of PTX alone.

5. Conclusions

In this study, the chemotherapeutic activity of the drug PTX was enhanced upon its encapsulation within small polymeric nanocapsules to develop a novel, less invasive, PTX nano-delivery system against malignant human ovarian carcinoma cells (SKOV-3). Frist, the average size of PTX-loaded polymer nanocapsules was approximately 18 nm and were colloidaly stable for long periods of time. Our *in vitro* cytotoxicity data revealed that lower concentrations of PTX-loaded polymeric nanocapsules lead to similar therapeutic activities than when administered the free drug. The results showed that 1 μg/mL polymer nanocapsules reduced IC50 of PTX from 14 to 2.2 μg/mL after 72 h of incubation, much lower that after the administration of the free drug. Interestingly, PTX-loaded polymer nanocapsules significantly increased apoptosis through caspase-dependent pathways and the cytoskeletal structure disruptions in the SKOV-3 cancer cells. Altogether, the present results highlighted the enhanced antiproliferative activity of PTX-loaded polymeric nanocapsules on SKOV-3 cancer cells and their potential as novel drug delivery vehicle to improve the therapeutic efficiency of the first line PTX administration in the treatment of ovarian cancer.

CRediT authorship contribution statement

Moein Golshan Ara: Investigation, Validation, Methodology, Formal analysis, Writing – original draft. **Gholamreza Motalleb:** Conceptualization, Formal analysis, Validation, Data curation, Methodology, Writing – original draft, Writing – review & editing. **Brenda Velasco:** Investigation, Formal analysis, Visualization. **Abbas Rahdar:** Conceptualization, Supervision, Writing – review & editing. **Pablo Taboada:** Formal analysis, Visualization, Funding acquisition, Writing – review & editing.

Declaration of Competing Interest

The authors declare that they have no known competing financial interests or personal relationships that could have appeared to influence the work reported in this paper.

Data availability

Data will be made available on request.

Acknowledgments

The University of Zabol, Islamic Republic of Iran, and Javid Biotechnology Company (JBC, Iran) are highly acknowledged. The authors are grateful to Dr. Asgari in the Javid Biotechnology Company (JBC, Iran). P.T. also thanks Agencia Estatal de Investigación (AEI) by project PID2019-109517RB-I00 and Xunta de Galicia ED431C 2022/18. ERDF funds are also acknowledged.

References

[1] A. Ashta, G. Motalleb, M. Ahmadi-Zeidabadi, Evaluation of frequency magnetic field, static field, and Temozolomide on viability, free radical production and gene expression (p53) in the human glioblastoma cell line (A172), Electromagn. Biol. Med. 39 (2020) 298–309, https://doi.org/10.1080/15368378.2020.1793171.

[2] P.A. Konstantinopoulos, B. Norquist, C. Lacchetti, D. Armstrong, R.N. Grisham, P. J. Goodfellow, E.C. Kohn, D.A. Levine, J.F. Liu, K.H. Lu, D. Sparacio, C. M. Annunziata, Germline and somatic tumor testing in epithelial ovarian cancer : ASCO Guideline, J. Clin. Oncol. 38 (2020) 1222–1245, https://doi.org/10.1200/JCO.19.02960.

[3] J.A. Ledermann, First-line treatment of ovarian cancer: questions and controversies to address. Therapeutic advances in medical, *Oncology* 10 (2018) 1–8, https://doi.org/10.1177/1758835918768232.

[4] M. Ramakrishna, L.H. Williams, S.E. Boyle, J.L. Bearfoot, A. Sridhar, T.P. Speed, K. L. Gorringe, I.G. Campbell, Identification of candidate growth promoting genes in ovarian cancer through integrated copy number and expression analysis, PLoS One 5 (2010) e9983.

[5] R. Pokhriyal, R. Hariprasad, L. Kumar, G. Hariprasad, Chemotherapy resistance in advanced ovarian cancer patients, Biomarkers in Cancer 11 (2019), https://doi.org/10.1177/1179299X19860815.

[6] B. Gao, F. Yang, W. Chen, R. Li, X. Hu, Y. Liang, D. Li, Multidrug resistance affects the prognosis of primary epithelial ovarian cancer, Oncol. Lett. 18 (2019) 4262–4269, https://doi.org/10.3892/ol.2019.10745.

[7] M.M. Gottesman, Mechanisms of cancer drug resistance, Ann. Rev. Med. 53 (2002) 615–627, https://doi.org/10.1146/annurev.med.53.082901.103929.

[8] M. Zeng, N.P. Kwiatkowski, T. Zhang, B. Nabet, M. Xu, Y. Liang, C. Quan, J. Wang, M. Hao, S. Palakurthi, S. Zhou, Q. Zeng, P.T. Kirschmeier, K. Meghani, A.L. Leggett, J. Qi, G.I. Shapiro, J.F. Liu, U.A. Matulonis, C.Y. Lin, P.A. Konstantinopoulos, N. S. Gray, Targeting MYC dependency in ovarian cancer through inhibition of CDK7 and CDK12/13, E-life 13 (2018) e39030. PMID: 30422115.

[9] H.M. Haikala, J.M. Anttila, E. Marques, T. Raatikainen, M. Ilander, H. Hakanen, H. Ala-Hongisto, M. Savelius, D. Balboa, B. Von Eyss, V. Eskelinen, P. Munne, A. I. Nieminen, T. Otonkoski, J. Schüler, Pharmacological reactivation of MYC-dependent apoptosis induces susceptibility to anti-PD-1 immunotherapy, Nature Commun. 10 (2019) 1–17, https://doi.org/10.1038/s41467-019-08541-2.

[10] P. Dutta, T. Bui, K.A. Bauckman, K. Keyomarsi, G.B. Mills, M. Nanjundan, EVI1 splice variants modulate functional responses in ovarian cancer cells, Mol. Oncol. 7 (2013) 647–668, https://doi.org/10.1016/j.molonc.2013.02.008.

[11] A.A. Jazaeri, J.S. Ferriss, J.L. Bryant, M.S. Dalton, A. Dutta, Evaluation of EVI1 and EVI1s (Δ324) as potential therapeutic targets in ovarian cancer, Gynecol. Oncol. 118 (2010) 189–195, https://doi.org/10.1016/j.ygyno.2010.04.007.

[12] Bleu, M., Mermet-Meillon, F., Apfel, V., Barys, L., Holzer, L., Salvy, M. B., Lopes, R., Barbosa, I. A. M., Delmas, C., Hinniger, A., Chau, S., Kaufmann, M., Haenni, S., Berneiser, K.,Wahle, M., oravec, I., Vissières, A., Poetsch, T., Ahrné, E., Carte, N., Voshol, J., Bechter, E., Hamon, J., Meyerhofer, M., Erdmann, D., Fischer, M., Stachyra, T., reuler, F., Gutmann , S., Fernández C., Schmelzle, T., Naumann, U., Roma G., Lawrenson K., Nieto-Oberhuber, C., Cobos-Correa, A., Stephane Ferretti, S., Schübeler, D. and Galli G. G. PAX8 and MECOM are interaction partners driving ovarian cancer. *Nature Commun.*, 12 (**2021**) 2442. Doi: 10.1038/s41467-021-22708-w.

[13] I. Hashimoto, K. Sakamaki, N. Oue, Y. Kimura, Y. Hiroshima, K. Hara, Y. Maezawa, K. Kano, T. Aoyama, T. Yamada, N. Yamamoto, T. Ogata, H. Ito, M. Shiozawa, S. Morinaga, Y. Rino, W. Yasui, M. Masuda, Y. Miyagi, T. Oshima, Clinical significance of PRKCI gene expression in cancerous tissue in patients with gastric cancer, Anticancer Res. 39 (2019) 5715–5720, https://doi.org/10.21873/anticanres.13771.

[14] L. Zhang, J. Huang, N. Yang, S. Liang, A. Barchetti, A. Giannakakis, M. G. Cadungog, A. O'Brien-Jenkins, M. Massobrio, K.F. Roby, D. Katsaros, P. Gimotty, R. Butzow, B.L. Weber, G. Coukos, Integrative genomic analysis of protein kinase C (PKC) family identifies PKCiota as a biomarker and potential oncogene in ovarian carcinoma, Cancer Res. 66 (2006) 4627–4635, https://doi.org/10.1158/0008-5472.can-05-4527.

[15] A.P. Fields, V. Justilien, N.R. Murray, The chromosome 3q26 OncCassette: A multigenic driver of human cancer, Adv. Biol. Regul. 60 (2016) 47–63, https://doi.org/10.1016/j.jbior.2015.10.009.

[16] P. Tran, J. Jang, S. Jeong, Y. Lee, Oral and Lymphatic Delivery of Paclitaxel via Lipid Nanocapsules, Yakhak Hoeji 65 (2021) 375–385, https://doi.org/10.17480/psk.2021.65.5.375.

[17] P. Kothamasu, H. Kanumur, N. Ravur, C. Maddu, R. Parasuramrajam, S. Thangavel, Nanocapsules: the weapons for novel drug delivery systems, Bioimpacts 2 (2012) 71–81, https://doi.org/10.5681/bi.2012.011.

[18] S. Deng, M.R. Gigliobianco, R. Censi, P. Di Martino, Polymeric Nanocapsules as Nanotechnological Alternative for Drug Delivery System: Current Status, Challenges and Opportunities, Nanomaterials (Basel) 28 (10) (2020) 847, https://doi.org/10.3390/nano10050847.

[19] S. Lukasiewicz, K. Szczepanowicz, K. Podgorna, E. Blasiak, N. Majeed, S.O. O. Ogren, W. Nowak, P. Warszynski, M. Dziedzicka-Wasylewska, Encapsulation of clozapine in polymeric nanocapsules and its biological effects, Colloids Surfaces B Biointerfaces 140 (2016) 342–352, https://doi.org/10.1016/j.colsurfb.2015.12.044.

[20] A.R. Pohlmann, V. Weiss, O. Mertins, N.P. Da Silveira, S.S. Guterres, Spray-dried indomethacin-loaded polyester nanocapsules and nanospheres: Development, stability evaluation and nanostructure models, Eur. J. Pharm. Sci 16 (2002) 305–312, https://doi.org/10.1016/S0928-0987(02)00127-6.

[21] S.L. Levit, H. Yang, C. Tang, Rapid self-assembly of polymer nanoparticles for synergistic codelivery of paclitaxel and lapatinib via flash nanoprecipitation, Nanomaterials 10 (2020) 561, https://doi.org/10.3390/nano10030561.

[22] M. Varshney, T.E. Morey, D.O. Shah, J.A. Flint, B.M. Moudgil, C.N. Seubert, D. M. Dennis, Pluronic microemulsions as nanoreservoirs for extraction of bupivacaine from normal saline, J. Am. Chem. Soc. 126 (2004) 5108–5112, https://doi.org/10.1021/ja0394479.

[23] A. Rahdar, P. Taboada, M.R. Hajinezhad, M. Barani, H. Beyzaei, Effect of tocopherol on the properties of Pluronic F127 microemulsions: Physico-chemical characterization and in vivo toxicity, J. Mol. Liq. 2019 (277) (2019) 624–630, https://doi.org/10.1016/j.molliq.2019.02.103.

[24] A. Rahdar, P. Hasanein, M. Bilal, H. Beyzaei, G.Z. Kyzas, Quercetin-loaded F127 nanomicelles: Antioxidant activity and protection against renal injury induced by gentamicin in rats, Life Sci. 1 (276) (2021), 119420, https://doi.org/10.1016/j.lfs.2021.119420.

[25] A. Rahdar, M. Almasi-Kashi, A.M. Khan, M. Aliahmad, A. Salimi, M. Guettari, H.E. G. Kohne, Effect of ion exchange in NaAOT surfactant on droplet size and location of dye within Rhodamine B (RhB)-containing microemulsion at low dye concentration, J. Mol. Liq 252 (2018) 506–513, https://doi.org/10.1016/j.molliq.2018.01.004.

[26] Taboada, P.; Velasquez, G.; Barbosa, S.; Castelletto, V.; Nixon, S. K.; Yang, Z.; Heatley, F. Hamley, I. W. Ashford, M.; Mosquera, V.; Attwood, D.; Booth, C. Block copolymers of ethylene oxide and phenyl glycidyl ether: Micellization, gelation, and drug solubilization. *Langmuir.* 21 (**2005**) 5263-5271. Doi: 10.1021/la0503808.

[27] Rahdar, A.; Hajinezhad, M.R.; Sargazi, S.; Barani, M.; Karimi, P.; Velasco, B.,; Taboada, P.; Pandey, S.; Bameri, Z.; Zarei, S. Pluronic F127/carfilzomib-based nanomicelles as promising nanocarriers: Synthesis, characterization, biological, and in silico evaluations. *J. Mol. Liq.* 346 (**2022**) 118271. Doi: 10.1016/j.molliq.2021.118271.

[28] K.S. Khashan, F.A. Abdulameer, M.S. Jabir, A.A. Hadi, G.M. Sulaiman, Anticancer activity and toxicity of carbon nanoparticles produced by pulsed laser ablation of graphite in water, Adv. Natural Sci.: Nanosci. Nanotechnol. 11 (3) (2020), 035010, https://doi.org/10.1088/2043-6254/aba1de.

[29] S. Sargazi, M.R. Hajinezhad, M. Barani, A. Rahdar, S. Shahraki, P. Karimi, M. Cucchiarini, M. Khatami, S. Pandey, Synthesis, characterization, toxicity and morphology assessments of newly prepared microemulsion systems for delivery of valproic acid, J. Mol. Liq. 2021 (338) (2021), 116625, https://doi.org/10.1016/j.molliq.2021.116625.

[30] K.J. Livak, T.D. Schmittgen, Analysis of relative gene expression data using real-time quantitative PCR and the 2(−Delta Delta C(T)) method, Methods 25 (4) (2001) 402–408, https://doi.org/10.1006/meth.2001.1262.

[31] T. Koressaar, M. Remm, Enhancements and modifications of primer design program Primer3, Bioinformatics 23 (2007) 1289–1291, https://doi.org/10.1093/bioinformatics/btm091.

[32] A. Untergasser, I. Cutcutache, T. Koressaar, J. Ye, B.C. Faircloth, M. Remm, S. G. Rozen, Primer3-new capabilities and interfaces, Nucleic Acids Res 40 (2012) e115–e, https://doi.org/10.1093/nar/gks596.

[33] J. Ye, G. Coulouris, I. Zaretskaya, I. Cutcutache, S.G. Rozen, T.L. Madden, Primer-BLAST: a tool to design target-specific primers for polymerase chain reaction, BMC Bioinf. 13 (2012) 134, https://doi.org/10.1186/1471-2105-13-134.

[34] O. Julien, J.A. Wells, Caspases and their substrates, Cell Death Differ. 24 (2017) 1380–1389, https://doi.org/10.1038/cdd.2017.44.

[35] A. Younus, S. Al-Ahmer, M. Jabir, Evaluation of some immunological markers in children with bacterial meningitis caused by Streptococcus pneumoniae, Res. J. Biotechnol. 14 (1) (2019) 131–133.

[36] S.L. Levit, H. Yang, C. Tang, Rapid self-assembly of polymer nanoparticles for synergistic codelivery of paclitaxel and lapatinib via flash nanoprecipitation, Nanomaterials 10 (3) (2020) 561, https://doi.org/10.3390/nano10030561.

[37] K. De Clercq, F. Xie, O. De Wever, B. Descamps, A. Hoorens, A. Vermeulen, W. Ceele, C. Vervat, Preclinical evaluation of local prolonged release of paclitaxel from gelatin microspheres for the prevention of recurrence of peritoneal carcinomatosis in advanced ovarian cancer, Sci. Rep. 9 (2019) 14881, https://doi.org/10.1038/s41598-019-51419-y.

[38] S. Nie, W.L. Hsiao, W. Pan, Z. Yang, Thermoreversible Pluronic F127-based hydrogel containing liposomes for the controlled delivery of paclitaxel: in vitro drug release, cell cytotoxicity, and uptake studies, Int. J. Nanomed. 6 (2011) 151–166, https://doi.org/10.2147/IJN.S15057.

[39] C.Y. Huang, C.M. Chen, Y.D. Lee, Synthesis of high loading and encapsulation efficient paclitaxel-loaded poly (n-butyl cyanoacrylate) nanoparticles via miniemulsion, Int. J. Pharm. 338 (2007) 267–275, https://doi.org/10.1016/j.ijpharm.2007.01.052.

[40] P. Ma, R.J. Mumper, Paclitaxel Nano-Delivery Systems: A Comprehensive Review, J. Nanomed. Nanotechnol. 4 (2) (2013) 1000164, https://doi.org/10.4172/2157-7439.1000164.

[41] Y. Su, J. Hu, Z. Huang, Y. Huang, B. Peng, N. Xie, H. Liu, Paclitaxel-loaded star-shaped copolymer nanoparticles for enhanced malignant melanoma chemotherapy against multidrug resistance, Drug Des. Develop. Ther. 6 (2017) 659–668, https://doi.org/10.2147/DDDT.S127328.
[42] H. Wang, Y. Jia, W. Hu, H. Jiang, J. Zhang, L. Zhang, Effect of preparation conditions on the size and encapsulation properties of mPEG-PLGA nanoparticles simultaneously loaded with vincristine sulfate and curcumin, Pharm. Devlop. Technol. 18 (3) (2013) 694–700, https://doi.org/10.3109/10837450.2012.696267.
[43] M. Brentnall, L. Rodriguez-Menocal, R.L. De Guevara, E. Cepero, L.H. Boise, Caspase-9, caspase-3 and caspase-7 have distinct roles during intrinsic apoptosis, BMC Cell Biol. 14 (2013) 32, https://doi.org/10.1186/1471-2121-14-32.
[44] J. Ahna, R. Biswas, J. Kim, The enhanced apoptotic effect of photodynamic therapy using photofrincombined with genistein in human ovarian cancer cell SK-OV-3, Biomed. Res.-Tokyo 25 (1) (2014) 51–57.
[45] H. Rehmani, Y. Li, T. Li, R. Padia, O. Calbay, L. Jin, H. Chen, S. Huang, Addiction to protein kinase Cι due to PRKCI gene amplification can be exploited for an aptamer-based targeted therapy in ovarian cancer, Signal Transduct. Target. Ther. 5 (2020) 140, https://doi.org/10.1038/s41392-020-0197-8.
[46] V. Justilien, M.P. Walsh, S.A. Ali, E.A. Thompson, N.R. Murray, A.P. Fields, The PRKCI and SOX2 oncogenes are coamplified and cooperate to activate Hedgehog signaling in lung squamous cell carcinoma, Cancer Cell 25 (2) (2014) 139–151, https://doi.org/10.1016/j.ccr.2014.01.008.
[47] X. Ren, B. Zhao, H. Chang, M. Xiao, Y. Wu, Y. Liu, Paclitaxel suppresses proliferation and induces apoptosis through regulation of ROS and the AKT/MAPK signaling pathway in canine mammary gland tumor cells, Mol. Med. Rep. 17 (2018) 8289–8299, https://doi.org/10.3892/mmr.2018.8868.
[48] N.C. Kampan, M.T. Madondo, O.M. McNally, M. Quinn, M. Plebanski, Paclitaxel and Its Evolving Role in the Management of Ovarian Cancer, BioMed. Res. Int. 2015 (2015), 413076, https://doi.org/10.1155/2015/413076.
[49] D. Zhang, R. Yang, S. Wang, Z. Dong, Paclitaxel: new uses for an old drug, Drug Des. Develop. Ther. 8 (2014) 279–284, https://doi.org/10.2147/DDDT.S56801.
[50] D.E. Lamendola, Z. Duan, R.Z. Yusuf, M.V. Seiden, Molecular Description of Evolving Paclitaxel Resistance in the SKOV-3 Human Ovarian Carcinoma Cell Line, Cancer Res. 63 (2003) 2200–2205.
[51] H. Wang, Y. Zhao, Y. Wu, Y. Hu, K. Nan, G. Nie, H. Chen, Enhanced anti-tumor efficacy by co-delivery of doxorubicin and paclitaxel with amphiphilic methoxy PEG-PLGA copolymer nanoparticles, Biomaterials 32 (2011) 8281–8290, https://doi.org/10.1016/j.biomaterials.2011.07.032.
[52] H.J. Ahn, Y.S. Kim, J. Kim, S.M. Han, J.W. Shin, H.O. Yang, Mechanism of Taxol-Induced Apoptosis in Human, J. Cell. Biochem. 91 (2004) 1043–1052, https://doi.org/10.1002/jcb.20006.
[53] L. Hamzehzadeh, A. Imanparast, A. Tajbakhsh, M. Rezaee, A. Pasdar, New Approaches to Use Nanoparticles for Treatment of Colorectal Cancer A Brief Review, *Nanomed. Res. J.* 1 (2016) 59–68, https://doi.org/10.7508/nmrj.2016.02.001.
[54] S. Elmore, Apoptosis: A Review of Programmed Cell Death, Toxicol. Pathol. 35 (4) (2007) 495–516, https://doi.org/10.1080/01926230701320337.
[55] Q. Han, J. Lu, J. Wang, J. Ye, X. Jiang, H. Chen, C. Liu, L. Chen, T. Lin, S. Chen, M. Sun, F. Gao, H2AFY is a novel fusion partner of MECOM in acute myeloid leukemia, Cancer Gen. 222–223 (2008) 9–12, https://doi.org/10.1016/j.cancergen.2018.01.004.
[56] E.A. Bard-Chapeau, J. Gunaratne, P. Kumar, B.Q. Chua, J. Muller, F.A. Bard, W. Blackstock, N.G. Copeland, N.A. Jenkins, EVI1 oncoprotein interacts with a large and complex network of proteins and integrates signals through protein phosphorylation, Proc. Natl. Acad. Sci. 110 (31) (2013) E2885–E2894, https://doi.org/10.1073/pnas.1309310110.
[57] K. Mitani, Molecular mechanisms of leukemogenesis by AML1/EVI-1, Oncogene 23 (2004) 4263–4269, https://doi.org/10.1038/sj.onc.1207777.
[58] S. Al-Dimassi, T. Abou-Antoun, M. El-Sibai, Cancer cell resistance mechanisms: a mini review, Clin. Transl. Oncol. 16 (2014) 511–516, https://doi.org/10.1007/s12094-014-1162-1.
[59] W.P. Tansey, Mammalian MYC Proteins and Cancer, New. J. Sci. 1–27 (2014), https://doi.org/10.1155/2014/757534.
[60] T.M. Abu Samaan, M. Samec, A. Liskova, P. Kubatka, D. Büsselberg, Paclitaxel's Mechanistic and Clinical Effects. *Biomolecules* 9 (2019) 789, https://doi.org/10.3390/biom9120789.
[61] P.P. Gan, J.A. McCarroll, S.A. Po'uha, K. Kamath, M.A. Jordan, M. Kavallaris, Microtubule Dynamics, Mitotic Arrest, and Apoptosis:Drug-Induced Differential Effects of βIII-Tubulin, Am. Assoc. Cancer Res. 9 (2010) 1339–1348, https://doi.org/10.1158/1535-7163.MCT-09-0679.
[62] E.M. Gordon, J.R. Ravicz, S. Liu, S.P. Chawla, F.L. Hall, Cell cycle checkpoint control: The cyclin G1/Mdm2/p53 axis emerges as a strategic target for broad–spectrum cancer gene therapy - A review of molecular mechanisms for oncologists, Mol. Clin. Oncol. 9 (2018) 115–134, https://doi.org/10.3892/mco.2018.1657.
[63] W.S. Ratnayake, C.A. Apostolatos, S. Breedy, A.H. Apostolatos, M. Acevedo-Duncan, FOXO1 regulates oncogenic PKC-ι expression in melanoma inversely to c-Jun in an autocrine manner via IL-17E and ICAM-1 activation, World Acad. Sci. J. 1 (2019) 25–38, https://doi.org/10.3892/wasj.2018.2.
[64] M.T. Hemann, S.W. Lowe, The p53–Bcl-2 connection, Cell Death & Differentation 13 (2006) 1256–1259, https://doi.org/10.1038/sj.cdd.4401962.
[65] M. Dong, G.C. Blobe, Role of transforming growth factor- in hematologic malignancies, Blood 107 (12) (2006) 4589–4596, https://doi.org/10.1182/blood-2005-10-4169.